Dynamic thermal model of passenger aircraft for the estimation of the cabin cooling and heating requirements

Giuffre', Andrea; Colonna, Piero; De Servi, Carlo

Important note
To cite this publication, please use the final published version (if applicable).
Please check the document version above.

Research Paper

Dynamic thermal model of passenger aircraft for the estimation of the cabin cooling and heating requirements

Andrea Giuffre' [a], Piero Colonna [a], Carlo De Servi [a,b,*]

[a] *Propulsion and Power, Delft University of Technology, Kluyverweg 1, Delft, 2629HS, The Netherlands*
[b] *Unit Energy Technology, Flemish Institute for Technological Research (VITO), Boeretang 200, Mol, 2400, Belgium*

ARTICLE INFO

ABSTRACT

The Environmental Control System (ECS) of passenger aircraft is the main consumer of non-propulsive power aboard. A computationally efficient and accurate thermal model of the fuselage is needed for future sustainable aircraft to address ECS preliminary sizing and control design, as the ECS should be re-designed to exploit possible synergies with other thermal management systems on board. Differently from previous works, the present aircraft thermal model is extensively documented and released open-source. Moreover, it is completely based on first principles and the acausal modeling paradigm. It results that the model is scalable, easily extendable, and allows for the estimation of the aircraft thermal loads given limited information about its configuration and flight mission. The predictive capabilities of the model have been assessed by comparing the thermodynamic state estimated at the pack discharge for three ECS operating points of an Airbus A320 with data provided by the manufacturer. The maximum deviation is limited to 2.4 K and 4.5 kPa. The validated thermal model has been used to compute the operating envelope of the A320 ECS, showing that the air supply requirements vary substantially with ambient conditions and flight phases. This calls for a multi-point design strategy when assessing novel ECS configurations.

1. Introduction

Modern commercial airliners fly at an altitude higher than eleven kilometers to reduce drag and fuel consumption. The environmental conditions at these altitude are incompatible with human life, due to the scarcity of oxygen, and the low pressure and temperature of the air. To make high-altitude flight possible, the Environmental Control System (ECS) is responsible for providing dry, sterile, and dust-free conditioned air to the airplane cabin at the proper temperature, flow rate, and pressure [1]. The technology of ECS's is well-established and very limited innovation has occurred in the last sixty years, with few exceptions, e.g., the bleedless air cycle machine equipping the Boeing 787 [2]. However, the assessment and improvement of the air quality in commercial aviation is still an active field of research and development, especially after the COVID-19 pandemic. Unlike other indoor spaces, the aircraft cabin is characterized by high occupant density, and the passengers are not allowed to leave the enclosed space for the entire duration of the flight mission. Moreover, in modern passenger aircraft, part of the pressurized air is filtered and recirculated in the air distribution system, instead of being entirely replenished by fresh air, to reduce the fuel consumption associated with the ECS. As a result, if not properly monitored, the concentration of gaseous and

microbiological contaminants may overcome the safety limits, leading to an increased probability of viral infections, and an exacerbation of chronic respiratory problems. Furthermore, the rapid changes in the cabin air pressure occurring during take-offs and landings may lead to ear and sinus problems, often accompanied by dental pain [3].

In addition to the safety and comfort concerns, the knowledge of the thermal loads associated with the prescribed environmental conditions within the aircraft's pressurized spaces is crucial for the correct sizing of the ECS. The ECS of modern passenger aircraft is designed not only to operate at nominal cruise conditions but also in other extreme atmospheric states, such as ground service on a hot and humid day. In this context, the availability of a model simulating the thermal characteristics of the pressurized aircraft compartments, i.e., cabin, cockpit, electronic and equipment (E/E) bay, and cargo bay, is essential to estimate the operating envelope of the ECS. This is testified by the various attempts to develop a thermal model for passenger aircraft documented in the scientific literature. In [4], the author presents a general overview of a one-dimensional Modelica thermal model developed at Airbus. As stated by the author, the objective of the work was to highlight the challenges related to providing a complete, accurate, and user-friendly thermal model of a complex thermal system, such as a

---

* Corresponding author at: Propulsion and Power, Delft University of Technology, Kluyverweg 1, Delft, 2629HS, The Netherlands.
E-mail addresses: a.giuffre@tudelft.nl (A. Giuffre'), p.colonna@tudelft.nl (P. Colonna), c.m.deservi@tudelft.nl (C. De Servi).

Nomenclature

Roman symbols

A	Surface area [m^2]
c	Specific heat capacity [J kg^{-1} K^{-1}]
c_P	Specific heat capacity at constant pressure [J kg^{-1} K^{-1}]
D	Diameter [m]
E	Irradiance [W m^{-2}] - Heat released by human body [W m^{-2} pax^{-1}]
g	Gravitational acceleration [m s^{-2}]
Gr	Grashof number [–]
H	Hour angle [deg]
h	Specific enthalpy [J kg^{-1}] - Hour of the day [–]
h_t	Heat transfer coefficient [W m^{-2} K^{-1}]
k_t	Thermal conductivity [W m^{-1} K^{-1}]
L	Length [m]
M	Metabolic heat production [W m^{-2}]
m	Mass [kg] - Relative air mass [–]
Ma	Mach number [–]
$\dot{m}$	Mass flow rate [kg s^{-1}]
$\dot{m}_{H2O}$	Rate of water vapor generation per person [kg s^{-1}pax^{-1}]
N	Number of elements [–]
n	Day of the year [–] - Refractive index [–]
Nu	Nusselt number [–]
Pr	Prandtl number [–]
$\dot{Q}$	Heat flow rate [W]
R	Radius [m] - Specific gas constant [J kg^{-1} K^{-1}]
r	Reflection coefficient [–]
Ra	Rayleigh number [–]
Re	Reynolds number [–]
T	Temperature [K]
t	Thickness [m] - Time [s]
U	Internal energy [J]
u	Specific internal energy [J kg^{-1}]
V	Velocity [ms^{-1}] - Volume [m^3]
W	Rate of mechanical work [W m^{-2}]
x	Mass fraction [–]
z	Altitude [m]

Greek symbols

α	Absorptivity [–]
β	Solar altitude angle [deg]
δ	Solar declination [deg]
ϵ	Emissivity [–]
Γ	Day correction [–]
γ	Surface-solar azimuth angle [deg]
μ	Dynamic viscosity [Pa s^{-1}]
v	Kinematic viscosity [m^2 s^{-1}]
Φ	Relative humidity [–] - Solar azimuth angle [deg]
ψ	Receiving surface azimuth angle [deg]
ρ	Density [kg m^{-3}] - Ground reflectance [–]
Σ	Tilt angle [deg]
σ	Boltzmann constant [m^2 kg s^{-2} K^{-1}]
τ	Location-specific irradiance coefficients - transmissivity [–]
θ	Incidence angle [deg]

Subscripts

abs	Absorbed component
amb	Ambient
av	Avionics
aw	Adiabatic wall
b	Direct beam component
cab	Cabin
cl	Cabin lights
conv	Convection
cpt	Cockpit
d	Diffuse component
diff	Water diffusion
el	Flight deck electronics
em	Emitted
ext	External
fus	Fuselage
gal	Galley
hb	Human body
i	Incident component
ife	In-flight entertainment
int	Internal
l	Liquid
lat	Latent
p	P-polarized light
pax	Passengers
r	Reflected component
rad	Radiation
rec	Recirculated
res	Respiration
rsw	Sweating
s	S-polarized light
sc	Solar constant
sens	Sensible
t	Component acting on the receiver surface
tot	Total
tr	Transmitted
ufloor	Underfloor
up	Unpolarized light
v	Vapor
w	Water

Abbreviations

AST	Apparent solar time
ET	Equation of time
LSM	Local standard meridian
LST	Local standard time

commercial aircraft, rather than to provide a detailed description of the proposed model. Similarly, the development and validation of a model used to size the ECS of passenger aircraft, named FLECS (Functional Model Library of the ECS), is documented in [5]. The article provides a list of data related to the considered aircraft configuration, but lacks a detailed description of the modeling approach, thus hindering the reproducibility of the model and its results. Another attempt to

CFD	Computational fluid dynamics
E/E	Electronics and equipment
ECS	Environmental control system
HEPA	High-efficiency particulate air
ISA	International standard atmosphere
LAT	Site latitude
LON	Site longitude
MSL	Mean sea level

devise a dynamic thermal model of the air distribution system and the pressurized compartments can be found in [6]. The authors investigated a new ducting concept, which enables the simultaneous control of many independent temperature zones. The focus of the article is on the rapid development of an efficient control strategy, obtained by coupling the Matlab and Modelica simulation environments. In particular, the design of the control logic was performed with Matlab, while Modelica was used to create a simplified thermal model of the pressurized aircraft compartments and to test the proposed control strategies. Further examples of one-dimensional thermal models developed for automotive applications are documented in [7,8]. An alternative approach to model the heat and mass transfer mechanisms occurring within the pressurized spaces of a commercial airliner is documented in [9]. In this paper, the authors rely on the results of high-fidelity Computational Fluid Dynamics (CFD) simulations to create fast and accurate reduced-order models. However, the proposed methodology is application-specific and requires the CFD simulation of each considered zone. As a consequence, it is deemed inappropriate for the purpose of this work.

The models documented in the aforementioned studies lack a detailed description of the underlying methodology and assumptions, hindering their reproducibility. Moreover, most of the cited works deal with specific applications and do not feature an exhaustive validation, which negatively affect the predictive capabilities of the model. Therefore, such models cannot be readily used outside the organization in which they have been developed and can be hardly extended to study the thermal management of other aircraft. To bridge such knowledge gap, the objective of this work is to develop a dynamic thermal model of the air distribution system and the pressurized compartments of a generic commercial aircraft, allowing for the estimation of the operating envelope of the ECS given limited information about the aircraft type and the flight mission. Such model should therefore satisfy the specific requirements of the preliminary design of the ECS and of its control strategy. The modeling library presented in this work, named *DynTherM* (Dynamic Thermal Management), has been designed to be scalable and easily extendable to cover additional thermal management applications relevant to the aerospace sector. To achieve these targets, it has been implemented in Modelica, i.e., an equation-based programming language created to simulate physical systems, supporting the acausal modeling paradigm [10] to facilitate modeling from first principles [11]. Moreover, it provides object-oriented constructs to facilitate the systematic reuse of models. The structure and the basic components of the *DynTherM* library are largely inspired by the *ThermoPower* library, i.e., an open-source Modelica library for the dynamic modeling of thermal power plants and energy conversion systems [12,13]. All the basic components of *DynTherM* are zero-dimensional, i.e., they do not feature a discretization of the governing physical equations in any spatial direction. To meet the objectives of reproducibility and open dissemination of knowledge, the *DynTherM* library and the aircraft thermal model documented in the following sections are released open-source under the GNU General Public License.

The remainder of the paper is structured as follows. First, the approach used to develop the thermal model is discussed and the main components of the *DynTherM* library are described. Next, a validation test case based on proprietary data provided by Airbus is documented.

Then, two different examples of usage of the aircraft thermal model are presented. Finally, concluding remarks summarize the content of the paper and provide an outlook of future work.

2. Methodology

2.1. System model

The air distribution system of a generic passenger aircraft is schematically displayed in Fig. 1. Two ECS packs, located in the unpressurized volume below the center wing box, provide conditioned and pressurized air to the mixing manifold. In the mixing unit, usually located under the cabin floor and in front of the center wing box, the fresh air is mixed with the recirculated cabin air. The recirculated air is extracted at the cabin floor level through dado panels, depurated by means of a high-efficiency particulate air (HEPA) filter, and fed to the mixing manifold with a recirculation fan. The aircraft is equipped with two recirculation loops located in the forward and aft sections of the cabin, for redundancy. Moreover, to guarantee a higher degree of temperature control, the aircraft cabin is divided into separate ventilation zones. The mixture of conditioned and recirculated air is distributed to the cockpit and to each cabin zone by means of dedicated supply ducts provided with orifices, and the mass flow rate is adjusted as a function of the temperature set points and of the corresponding heat loads. Furthermore, the air temperature is regulated by mixing hot trim air, bled from the compressors of the main engines, with the air stream coming from the mixing unit. To fine-tune the local air temperature, the flow rate of trim air is controlled by means of a separate trim-air valve installed in each zone. In addition, the air distribution system provides ventilation to the cargo and the electronics (E/E) bays, by means of dado panels located on the floor of the cabin and cockpit, respectively. The pressurization level is regulated by the opening of the outflow valves positioned in the forward and aft cargo compartments, as a function of the altitude.

To describe the modeling approach adopted in this work, it is convenient to analyze the heat and mass transfer processes occurring within one section of the fuselage, which corresponds to one ventilation zone, as depicted in Fig. 2. From the outer to the inner surface, the overall heat transfer can be decomposed into the following contributions:

- external radiative and convective heat transfer established between the environment and the outer skin of the fuselage;
- heat conduction through the fuselage composite structure;
- radiative and convective heat transfer between the fuselage inner surface and the pressurized air volume.

The temperature difference between the fuselage interior and the pressurized air volume is negligible, due to the presence of an insulation layer within the fuselage composite structure. Moreover, the temperature is low, since it is directly regulated by the ECS. As a result, the internal radiative heat transfer can be neglected as a first approximation. Additional heat transfer mechanisms must be accounted for due to the presence of cabin windows and cockpit windshields. The external radiative heat transfer is subdivided into the absorbed, transmitted, and reflected components. The transmitted component is directed to the cabin and cockpit interiors. This thermal power is then partly transferred to the surrounding air by convection.

Furthermore, the following processes involving mass transfer take place within the prescribed fuselage section:

- a mixture of fresh, recirculated, and trim air is supplied to the prescribed ventilation zone by the air distribution system;
- mass transfer occurs between the upper and lower sections of the fuselage by means of the dado panels located on the cabin floor;
- part of the air in the cargo bay is vented overboard by means of the outflow valve and the rest is fed to the recirculation loop.
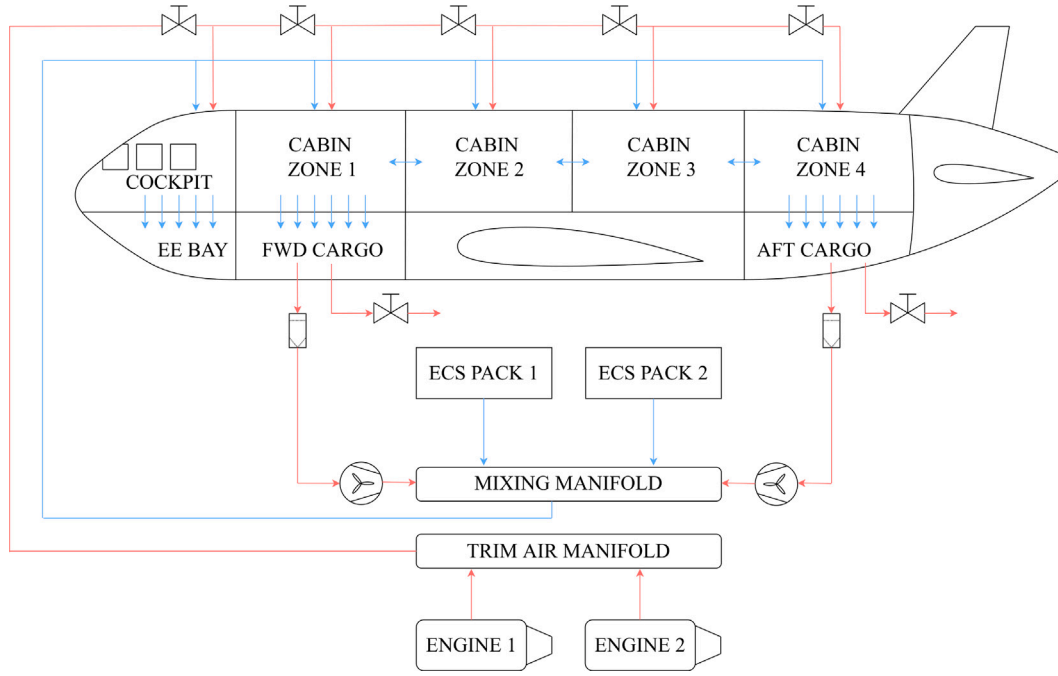
Fig. 1. Simplified schematic of the air distribution system of an exemplary passenger aircraft.

The model of the entire fuselage can be assembled by coupling together multiple sections, characterized by the heat and mass transfer processes described above. Following this approach, each instance corresponds to a separate ventilation zone. The cockpit and the E/E bay can be modeled in the same fashion as the cabin and cargo compartments, with only minor modifications, accounting for the variation of the shape of the fuselage, the presence of larger transparencies in the cockpit, and the internal heat loads due to the flight deck electronics and avionics. This modeling approach complies with the requirements of the development of a library featuring a modular structure, as displayed in Fig. 3. In the current implementation, the lowest hierarchical layer, labeled as utilities, collects the packages defining the interfaces of each component and the boundary conditions used for the simulations. Moreover, it gathers the material properties and the sensors. The intermediate layer contains the implementation of the basic components. These are organized in two packages, collecting the models related to heat and mass transfer. Moreover, a model to predict the atmospheric conditions, called environment, is included in the intermediate layer. Finally, the models of the aircraft and the related subsystems are collected within the top hierarchical layer. In particular, the packages of the aircraft subsystems are organized into three levels featuring an increasing degree of complexity and inheritance. Following the notation of Fig. 3, the package SubSystems L1 collects the models of the composite structures of the fuselage, cabin floor, and wall. Moreover, it includes the model of the transparent surfaces. In Subsystems L2, the models of the composite structures and the windows are coupled to those of convective and radiative heat transfer to create the building blocks of the upper and lower fuselage. At the third level, the models of the pressurized aircraft compartments are created by assembling multiple instances of the upper and lower fuselage, featuring different orientations. Finally, the air distribution system is modeled by resorting to the components of the mass transfer package, and the model of the aircraft is created by connecting the third-level subsystems. This modular modeling approach is illustrated in Figs. 4 and 5.

The total mass, air species (mass fractions), and energy conservation equations applied to the pressurized air volume of one ventilation zone within the fuselage read

$$\frac{\mathrm{d}m}{\mathrm{d}t} = V \cdot \frac{\mathrm{d}\rho}{\mathrm{d}t} = \dot{m}_{\mathrm{in}} + \dot{m}_{\mathrm{out}} + N_{\mathrm{pax}}\dot{m}_{\mathrm{H_2O}}, \tag{1}$$

$$\frac{\mathrm{d}U}{\mathrm{d}t} = V \cdot \frac{\mathrm{d}(\rho u)}{\mathrm{d}t} = \dot{m}_{\mathrm{in}}h_{\mathrm{in}} + \dot{m}_{\mathrm{out}}h_{\mathrm{out}} + \dot{Q}_{\mathrm{in}} + \dot{Q}_{\mathrm{out}} +$$
$$+ N_{\mathrm{pax}}(\dot{Q}_{\mathrm{sens}} + \dot{Q}_{\mathrm{lat}}) + \dot{Q}_{\mathrm{int}}, \tag{2}$$

$$m \cdot \frac{\mathrm{d}x_{\mathrm{w}}}{\mathrm{d}t} = \dot{m}_{\mathrm{in}}(x_{\mathrm{in,w}} - x_{\mathrm{w}}) + \dot{m}_{\mathrm{out}}(x_{\mathrm{out,w}} - x_{\mathrm{w}}) +$$
$$+ N_{\mathrm{pax}}\dot{m}_{\mathrm{H_2O}}(1 - x_{\mathrm{w}}),$$

$$m \cdot \frac{\mathrm{d}x_{\mathrm{air}}}{\mathrm{d}t} = \dot{m}_{\mathrm{in}}(x_{\mathrm{in,air}} - x_{\mathrm{air}}) + \tag{3}$$
$$+ \dot{m}_{\mathrm{out}}(x_{\mathrm{out,air}} - x_{\mathrm{air}}) - N_{\mathrm{pax}}\dot{m}_{\mathrm{H_2O}}x_{\mathrm{air}},$$

$$x_{\mathrm{w}} + x_{\mathrm{air}} = 1.$$

The heat flow rate terms which, once summed up, give the total internal heat flow rate $\dot{Q}_{\mathrm{int}}$ depend on the considered ventilation zone. In the case of a cabin sector, the terms are the heat flow rate associated with the cabin lights, that related to the in-flight entertainment, and the heat flow rate provided by the galleys. Conversely, for the cockpit and the related underfloor compartment, i.e., the E/E bay, the sources of internal heat flow rate are the flight deck electronics and the avionics.

The presence of occupants, i.e., pilots (cockpit), passengers, and crew members (cabin), leads to the generation of water vapor within the pressurized air volume. As reported in [14], the rate of evaporative heat generation from the human body can be expressed as

$$E_{\mathrm{hb}} = E_{\mathrm{rsw}} + E_{\mathrm{diff}} + E_{\mathrm{res}}, \tag{4}$$

where E_{rsw}, E_{diff}, and E_{res} are the rates of heat generation due to sweating, water diffusion through the skin, and respiration, respectively. They can be computed as

$$E_{\mathrm{rsw}} = 0.42(M_{\mathrm{hb}} - W_{\mathrm{hb}} - 58.15),$$
$$E_{\mathrm{diff}} = 3.05(5.73 - 0.007(M_{\mathrm{hb}} - W_{\mathrm{hb}}) - P_{\mathrm{v}}/1000), \tag{5}$$
$$E_{\mathrm{res}} = 0.0173M_{\mathrm{hb}}(5.87 - P_{\mathrm{v}}/1000),$$

where P_{v} is the water vapor pressure in the pressurized air volume, whereas M_{hb} and W_{hb} are the rate of metabolic heat production and the rate of mechanical work accomplished by one individual, respectively. According to the guidelines reported in [15], M_{hb} can be set to 60, 115, and 70 W m^{-2} for passengers, crew members, and pilots, respectively. Moreover, as a first approximation, W_{hb} can be neglected. The rate of
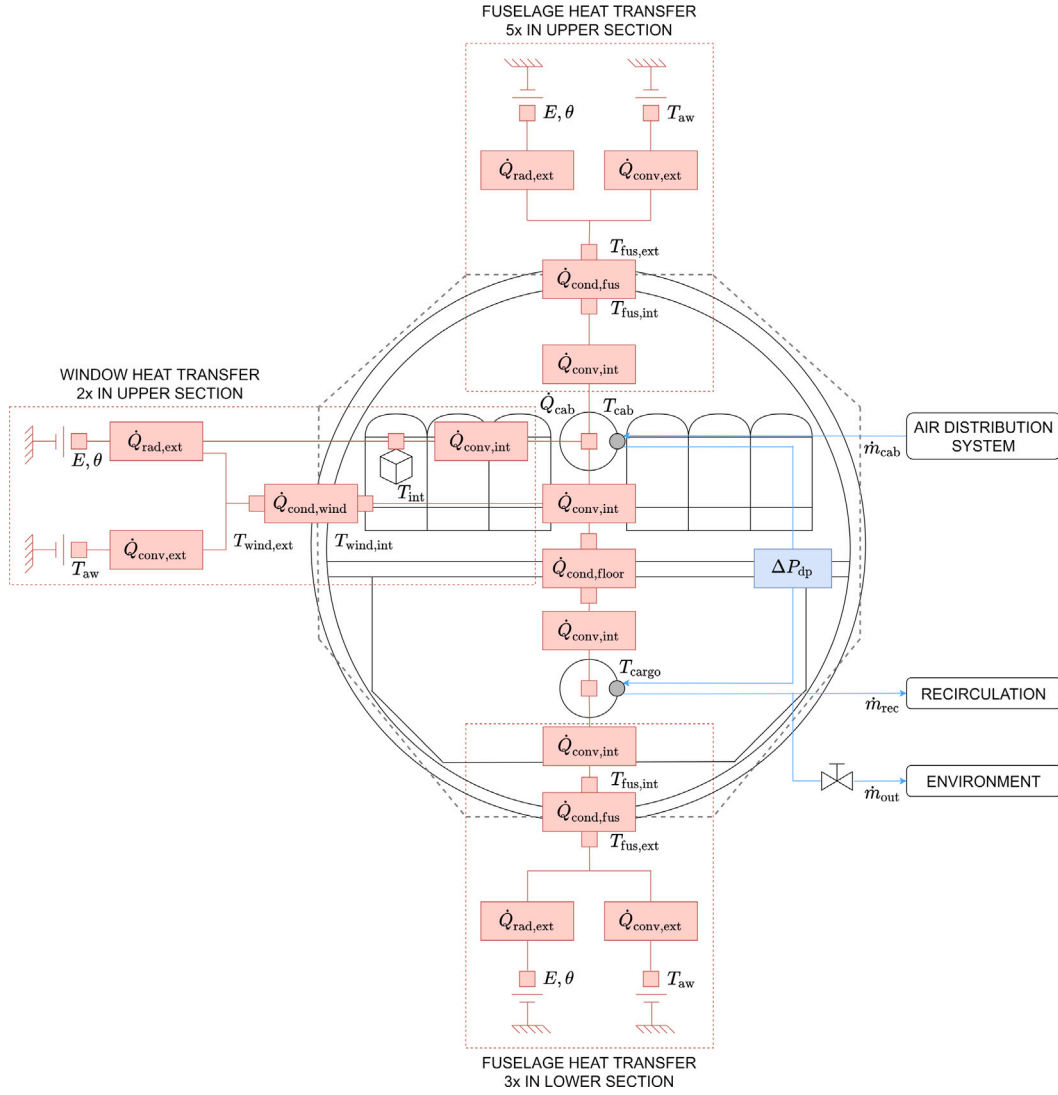
Fig. 2. Diagram of the model decomposition of the heat and mass transfer processes occurring in one section of the fuselage, corresponding to one ventilation zone.

water vapor generation per person can be calculated by considering the average surface area of the human body, i.e., $A_{hb} = 1.75$ m^2, and the rate of the evaporative heat loss

$$\dot{m}_{H_2O} = \frac{E_{hb} A_{hb}}{h_v(T) - h_l(T_{skin})}. \tag{6}$$

In Eq. (6), T is the temperature of the pressurized air volume, and T_{skin} is the skin temperature of the human body, estimated as reported in [16]

$$T_{skin} = 273.15 + 37.5 - 0.0275(M_{hb} - W_{hb}). \tag{7}$$

The sensible and latent components of the heat flow rate associated with the generation of water vapor in the prescribed air volume can be computed as

$$\dot{Q}_{sens} = A_{hb} \cdot (M_{hb} - E_{hb}), \tag{8}$$

$$\dot{Q}_{lat} = \dot{m}_{H_2O}(h_v(T) - h_l(T_{skin})). \tag{9}$$

The pressurized air volumes of the upper and lower fuselage sections, i.e., cabin and cargo, or cockpit and E/E bay, exchange heat and mass through the dado panels and the cabin floor. Furthermore, the cabin and the cockpit sections exchange energy as heat via the wall separating the two environments. The dado panels are modeled

as simple elements featuring a lumped pressure drop, that scales linearly with the mass flow rate of air. The floor and the wall are heat conduction elements featuring a planar composite structure. The cabin can be discretized into multiple ventilation zones connected in series, without additional modeling effort, by leveraging the modularity of the *DynTherM* library. However, for the sake of simplicity, the cabin is assumed to be constituted by a single ventilation zone. To keep the internal pressure at the prescribed set point value, part of the air in the underfloor compartment is vented overboard by means of the outflow valve. In the current implementation, the valve features a simple linear characteristic. The remaining airflow is fed to the recirculation loop, amounting to the HEPA filter, the recirculation fan, and the mixing manifold. These components are modeled as a pressure drop, a turbomachine with a linear characteristic, and a plenum featuring accumulation of mass and energy. Finally, the mix of fresh and recirculated air at the outlet of the mixing manifold is provided to each ventilation zone by means of a separate distribution pipe. The pressure drop in the air distribution system is modeled with the Darcy-Weisbach equation and the heat transfer is neglected, due to the thick thermal insulation. The graphical representation of the complete model of a passenger aircraft featuring two ventilation zones, i.e., cockpit and cabin, is depicted in Fig. 5.
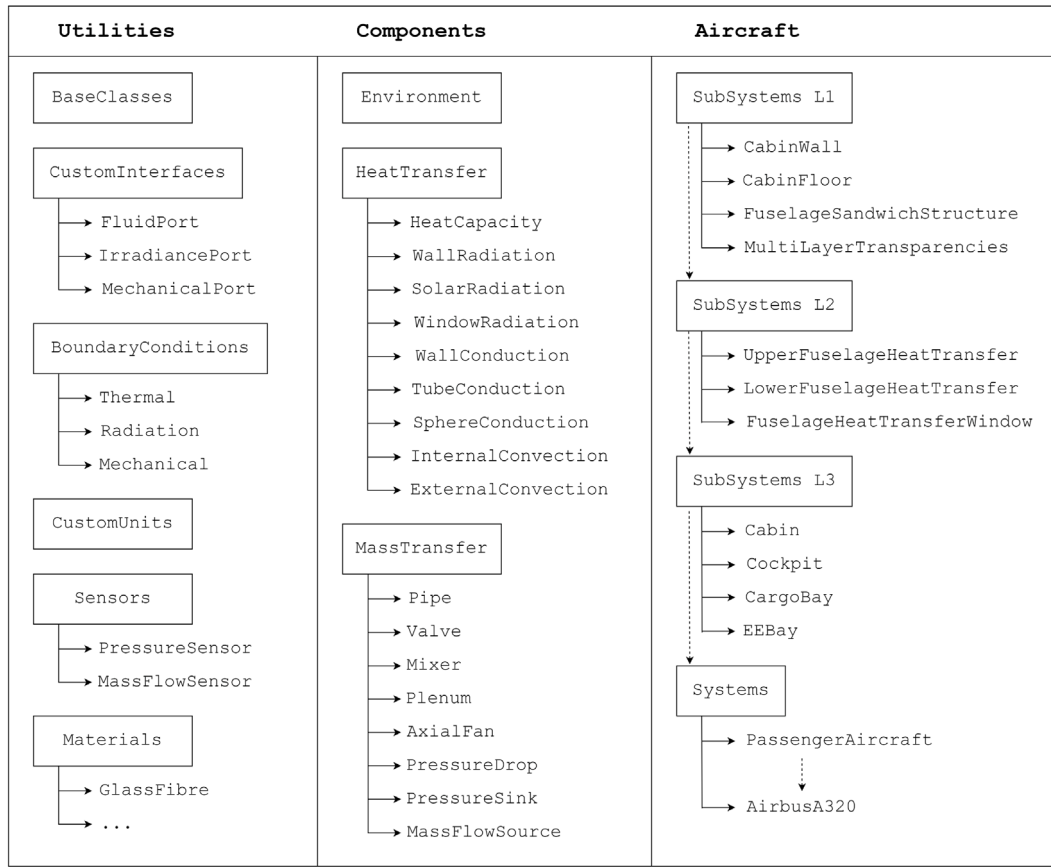
Fig. 3. Structure of the *DynTherM* Modelica library. The solid arrows indicate the list of models collected within a package. The dashed arrows indicate model inheritance.

2.2. Model of external environment

The International Standard Atmosphere (ISA) [17] is used to model the variation of the atmospheric conditions with altitude. Within this model, the atmosphere is divided into layers, in which the ambient temperature is computed as a function of altitude. In particular, until the Tropopause, located at eleven kilometers above Mean Sea Level (MSL), the ambient temperature is evaluated as

$$T_{\text{ISA}} = T_0 - \frac{6.5z}{1000},\tag{10}$$

where $T_0 = 15°$ C is the average ambient temperature at MSL and z is the altitude. Then, between the Tropopause and the edge of the Stratosphere, located at 20 kilometers above MSL, the ambient temperature is assumed to be constant and equal to $T_{\text{ISA}} = -56.5°$ C. The ambient pressure and density are computed by sequentially solving the hydrostatic equilibrium, which relates the rate of change of pressure with geopotential altitude, and the ideal gas law, therefore

$$P_{\text{ISA}} = P_0 \frac{T_{\text{ISA}}}{T_0}^{\frac{1000g}{6.5R}} \quad \text{if } z \leq 11 \text{ km},$$

$$P_{\text{ISA}} = P_0 \frac{T_{\text{ISA}}}{T_0}^{\frac{1000g}{6.5R}} e^{-\frac{g}{T_{\text{ISA}}R}(z-11000)}$$

$$\text{if } 11 \text{ km} < z \leq 20 \text{ km},$$

$$\rho_{\text{ISA}} = \frac{P_{\text{ISA}}}{T_{\text{ISA}}R},\tag{11}$$

where $P_0 = 1$ bar is the ambient pressure at MSL. In the ISA model, the ambient air is assumed to be dry and of constant composition. Humidity effects are accounted for by adopting a standard moist air thermodynamic model in which the air pressure and temperature are defined according to the ISA model. Non-standard days are modeled by adding a prescribed temperature delta to T_{ISA}, whereas the ambient pressure remains unaltered. Then, density is recalculated as a function of the new ambient temperature using the ideal gas equation of state. Once the ambient conditions are defined, the set-point pressure of the pressurized spaces of the aircraft can be computed by imposing a maximum pressure differential of 50 kPa with respect to the external environment. Moreover, for safety reasons, the minimum pressure within the ventilation zones is fixed at 76.2 kPa.

In addition to the standard atmospheric conditions, the model of the environment is used to compute the clear-sky temperature and emissivity, which are used for the radiative heat transfer calculation, as described in Section 2.5. The vapor pressure of ambient air is computed according to [18] as

$$P_v = \Phi_{\text{amb}} e^{\frac{29.06 - 6211.88}{T_{\text{amb}}} + 274.35} \quad \text{if } T_{\text{amb}} < 0° \text{ C},$$

$$P_v = \Phi_{\text{amb}} e^{\frac{23.3 - 3890.94}{T_{\text{amb}}} + 230.4} \quad \text{if } T_{\text{amb}} \geq 0° \text{ C},\tag{12}$$

with T_{amb} expressed in Celsius. The clear-sky temperature and emissivity can be derived as reported in [19]

$$\epsilon_{\text{sky}} = \left(0.48 + 0.17 \left(\frac{P_v}{100}\right)^{0.22}\right) \left(\frac{P_{\text{amb}}}{P_0}\right)^{0.45}$$

$$\text{if } T_{\text{amb}} < 0° \text{ C},$$

$$\epsilon_{\text{sky}} = \left(\frac{T_{\text{sky}}}{T_{\text{amb}}}\right)^4 \quad \text{if } T_{\text{amb}} \geq 0° \text{ C}.\tag{13}$$

2.3. Model of composite structures

The geometry of the composite structures of a passenger aircraft can be approximated with two simple geometries, i.e., a planar element, and a hollow cylinder. The planar element is used to model the cabin
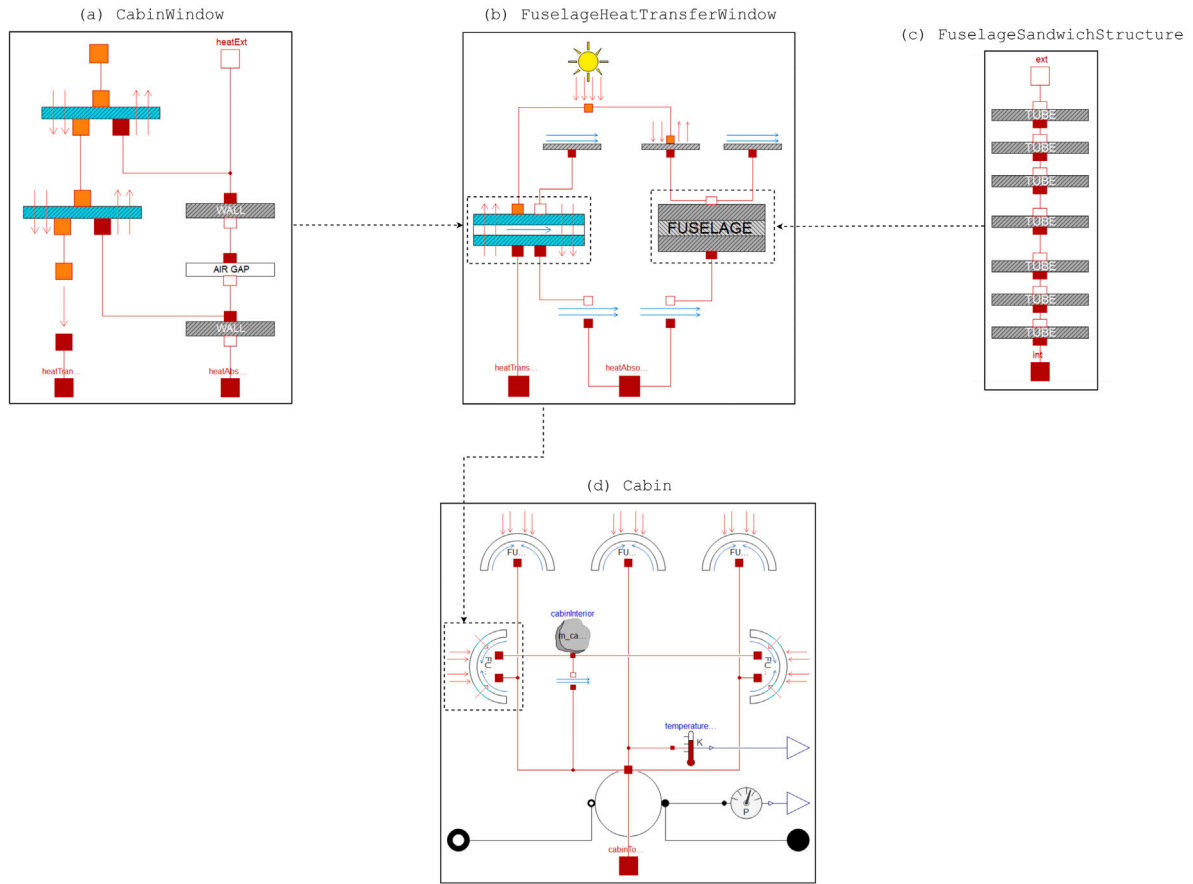
Fig. 4. Graphical user interface of the Modelica model of the aircraft cabin and its main submodels, as implemented in the *DynTherM* library. The dashed arrows indicate the usage of a submodel in a higher hierarchical layer.

Fig. 5. Graphical user interface of the Modelica model of a passenger aircraft and its main submodels, as implemented in the *DynTherM* library. The dashed arrows indicate the usage of a submodel in a higher hierarchical layer.
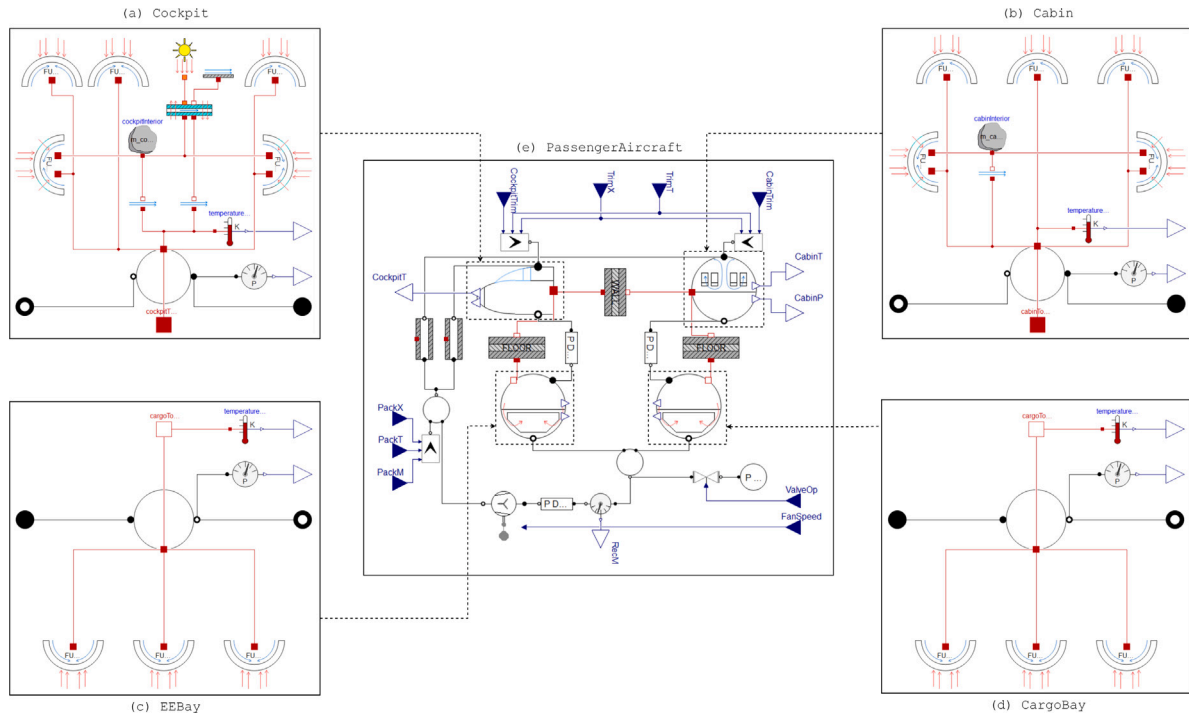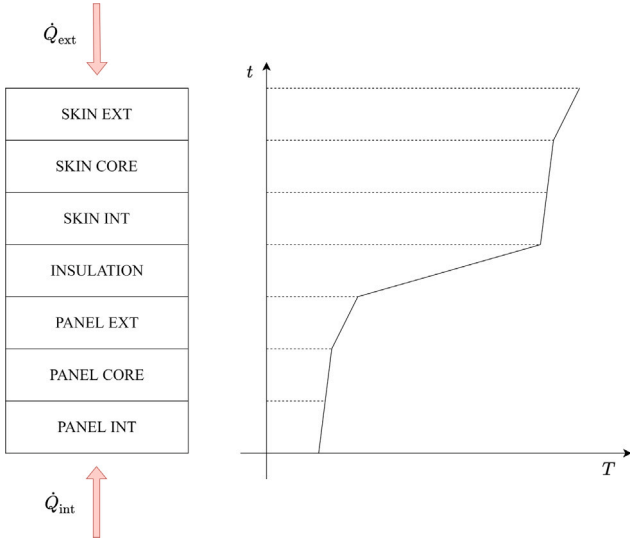
Fig. 6. Heat conduction and qualitative temperature distribution evaluated through the layers of the fuselage composite structure.

floor and the wall separating the cockpit from the cabin. The heat conduction equations for a planar surface of thickness t reads

$$
\dot{Q}_{\text{in}} = \frac{2k_t A(T_{\text{in}} - T)}{t},
$$
$$
\dot{Q}_{\text{out}} = \frac{2k_t A(T_{\text{out}} - T)}{t}. \tag{14}
$$

The hollow cylinder is used to model the fuselage structure in between the forward and aft pressure bulkheads. The thermal energy balance equations for the heat conduction in a hollow cylindrical section can be expressed as

$$
\dot{Q}_{\text{in}} = \frac{2\pi L_{\text{fus}} k_t (T_{\text{in}} - T)}{\log \frac{R_{\text{int}} + R_{\text{ext}}}{2R_{\text{int}}}},
$$
$$
\dot{Q}_{\text{out}} = \frac{2\pi L_{\text{fus}} k_t (T_{\text{out}} - T)}{\log \frac{2R_{\text{ext}}}{R_{\text{int}} + R_{\text{ext}}}}. \tag{15}
$$

The surface areas occupied by transparent surfaces, e.g., cabin windows, are excluded from this computation, as they are characterized by different physical properties and heat transfer mechanisms. Further information about the methodology used to model the heat transfer mechanisms for transparent surfaces is described in Section 2.4. Once the heat conduction mechanisms characterizing the two basic geometries have been derived, the corresponding composite structures can be modeled by connecting in series multiple planar or cylindrical elements, featuring different dimensions and material properties, as displayed in Fig. 4c and Fig. 6. With reference to Fig. 6, the inner and outer boundaries of the composite structure are exposed to $\dot{Q}_{\text{int}}$ and $\dot{Q}_{\text{ext}}$, respectively, which can be either entering or leaving the control volume depending on the net convective and radiative heat transfer at the boundary. In turn, this influences the actual temperature distribution within the composite structure. In the scenario qualitatively depicted in the Figure, the temperature of the outer skin is higher than that of the internal panel facing the cabin interior. This is representative, for example, of a ground operation during a hot day.

2.4. Model of transparent surfaces

The external surface of the fuselage of a passenger aircraft features two types of transparencies: cabin windows and flight deck windshields. Cabin windows consist of an outer panel flush with the fuselage skin, an inner panel featuring a breather hole, and a thinner non-structural scratch panel, separating the passengers from the actual

window assembly. The scratch panel is made of plastic and is not airtight. The inner and outer panels are made of stretched acrylic, and feature a non-ventilated air cavity between them. During the climb phase, the pressure differential established between the interior of the fuselage and the external environment gradually increases. The breather hole on the inner panel allows some of the pressurized air to leak into the air cavity, gradually equalizing the pressure differential. This causes the thicker outer panel to progressively carry the pressurization load, whereas the inner panel acts only as a buffer.

The model of the heat transfer through the cabin windows is adapted from [20] and its graphical representation is illustrated in Fig. 4a. The solar radiation acting on the outer panel is split into the absorbed, transmitted, and reflected components, yielding

$$
E_{\text{r}} = (r_{\text{up}} + r_{\text{up}}(1 - r_{\text{up}})\tau^2)E_{\text{t,b}},
$$
$$
E_{\text{tr}} = (1 - r_{\text{up}})^2 \tau E_{\text{t,b}}, \tag{16}
$$
$$
E_{\text{abs}} = E_{\text{t,b}} - E_{\text{r}} - E_{\text{tr}}.
$$

If $\cos\theta \leq 0$, the incident solar radiation is entirely reflected by the surface, leading to $E_{\text{tr}} = E_{\text{abs}} = 0$. The reflection coefficient r_{up} can be computed by applying the Snell's law

$$
n_1 \sin\theta_{\text{i}} = n_2 \sin\theta_{\text{tr}}, \tag{17}
$$

and the Fresnel equations

$$
r_{\text{s}} = |\frac{n_1 \cos\theta_{\text{i}} - n_2 \cos\theta_{\text{tr}}}{n_1 \cos\theta_{\text{i}} + n_2 \cos\theta_{\text{tr}}}|,
$$
$$
r_{\text{p}} = |\frac{n_1 \cos\theta_{\text{tr}} - n_2 \cos\theta_{\text{i}}}{n_1 \cos\theta_{\text{tr}} + n_2 \cos\theta_{\text{i}}}|, \tag{18}
$$

at the interface between the external air and the outer panel. In this case, subscript 1 corresponds to the air side, and subscript 2 refers to the stretched acrylic side. Moreover, r_{s} and r_{p} are the reflection coefficients computed for s-polarized and p-polarized light. r_{s} refers to the polarization of a wave's electric field normal to the plane of incidence, whereas r_{p} refers to the polarization of the electric field parallel to the plane of incidence. Unpolarized natural light has an equal amount of power in each of the two linear polarizations, thus its reflection coefficient can be simply estimated as $r_{\text{up}} = (r_{\text{s}} + r_{\text{p}})/2$.

The absorbed component of the incident solar radiation contributes to the conductive heat balance through the outer panel, which is modeled as a planar element, according to the method described in Section 2.3. The convective heat transfer coefficient in the air cavity is computed according to the correlation documented in [21], namely

$$
h_{\text{t}} = \frac{Nu \cdot k_t}{t}, \tag{19}
$$

where t is the thickness of the air cavity, the Nusselt number is evaluated as

$$
Nu = 0.0673838 \cdot Ra^{1/3} \quad \text{if } Ra > 5 \cdot 10^4,
$$
$$
Nu = 0.028154 \cdot Ra^{0.4134} \quad \text{if } 10^4 < Ra \leq 5 \cdot 10^4, \tag{20}
$$
$$
Nu = 1 + 1.75967 \cdot 10^{-10} \cdot Ra^{2.2984755} \quad Ra \leq 10^4,
$$

while the Rayleigh number is computed as

$$
Ra = \rho^2 t^3 \ g \frac{2c_{\text{P}}|T_{\text{in}} - T_{\text{out}}|}{\mu k_t (T_{\text{in}} + T_{\text{out}})}. \tag{21}
$$

The transmitted component of the incident radiation acts directly on the inner panel. Therefore, the computation described by Eq. (18) is repeated, accounting for the change of media at the interface. The heat transfer mechanisms established in the inner panel are equivalent to those acting on the outer panel. As a result, also the modeling approach is the same. However, in the case of the inner panel the transmitted component of radiation contributes to the heat balance of the cabin interiors.

Flight deck windshields are made of glass-faced acrylic, i.e., an outer layer of glass bonded to one or multiple layers of stretched acrylic. In between the glass and the acrylic, there is a thin urethane layer. The

stretched acrylic layers are equivalent to the ones of the cabin windows, albeit much thicker. The methodology used to model the heat transfer through the flight deck windshields is the same as the one adopted for the cabin windows, with minor modifications due to the presence of multiple layers and the absence of the air gap. Therefore, the detailed description of the windshield model is omitted here for the sake of conciseness.

2.5. Fuselage model

The heat flow rate due to solar radiation acting on the outer skin of the fuselage scales as a function of the total clear-sky irradiance impinging on the receiving surface E_t and the incidence angle θ. In particular, the total irradiance is the sum of the direct beam, diffuse, and ground-reflected components. These quantities can be estimated with the methodology documented in [22,23] and reported in Appendix A. As an alternative, they can be computed by means of external software implementing more advanced algorithms, such as the open-source program SMARTS [24–26]. In turn, the incidence angle depends on the sun position in the sky, and the altitude and orientation of the receiver, i.e., the fuselage, see Fig. 7. To capture the variation of the incidence angle along the circumferential direction, the fuselage section can be conveniently discretized as a series of circular sectors featuring different orientations. In this way, the average orientation of each sector is equivalent to that of the associated segment, as represented by the dashed lines in Fig. 2c. Each circular sector is characterized by the composite structure described in Section 2.3, and is subject to

$$\dot{Q}_{\text{rad}} = \dot{Q}_{\text{abs}} + \dot{Q}_{\text{em}}, \tag{22}$$

where

$$\begin{aligned} \dot{Q}_{\text{abs}} &= -\alpha A E_t, \\ \dot{Q}_{\text{em}} &= \dot{Q}_{\text{em,sky}} + \dot{Q}_{\text{em,air}} + \dot{Q}_{\text{em,ground}}. \end{aligned} \tag{23}$$

In particular, the different components of the emitted radiation can be expressed as [27]

$$\begin{aligned} \dot{Q}_{\text{em,sky}} &= \epsilon A \sigma \left(\frac{1 + \cos \Sigma}{2} \right)^{3/2} \left(T_{\text{fus,ext}}^4 - T_{\text{sky}}^4 \right), \\ \dot{Q}_{\text{em,air}} &= \epsilon A \sigma \frac{1 + \cos \Sigma}{2} \left(1 - \sqrt{\frac{1 + \cos \Sigma}{2}} \right) \cdot \\ &\quad \cdot \left(T_{\text{fus,ext}}^4 - T_{\text{amb}}^4 \right), \\ \dot{Q}_{\text{em,ground}} &= \epsilon A \sigma \frac{1 - \cos \Sigma}{2} \left(T_{\text{fus,ext}}^4 - T_{\text{ground}}^4 \right). \end{aligned} \tag{24}$$

For the sake of clarity, the different components contributing to the radiative heat transfer between the fuselage and the external environment are schematically displayed in Fig. 8. In addition to the variation of the incidence angle along the circumferential direction, the orientation of the fuselage with respect to the sun position and the intensity of the solar irradiance vary as a function of time. To account for this effect, it is necessary to model the aircraft mission, by providing the variation over time of the aircraft altitude and orientation. This is disregarded in the present analysis for the sake of simplicity. However, the case studies analyzed in Section 3 and Section 4 are characterized by either steady-state calculations or transient analysis related to stationary aircraft operation featuring a short duration. Therefore, the results reported in the following are not affected by this approximation.

In addition to solar radiation, each circular sector is subject to convection heat transfer from the inside and from the outside. According to the guidelines reported in [28], the physical mechanism driving the convective heat transfer between the outer skin of the fuselage and the environment depends on the flight phase and the environmental conditions. During flight, the cold ambient air adjacent to the outer skin of the aircraft is heated through the ram effect. Given that the
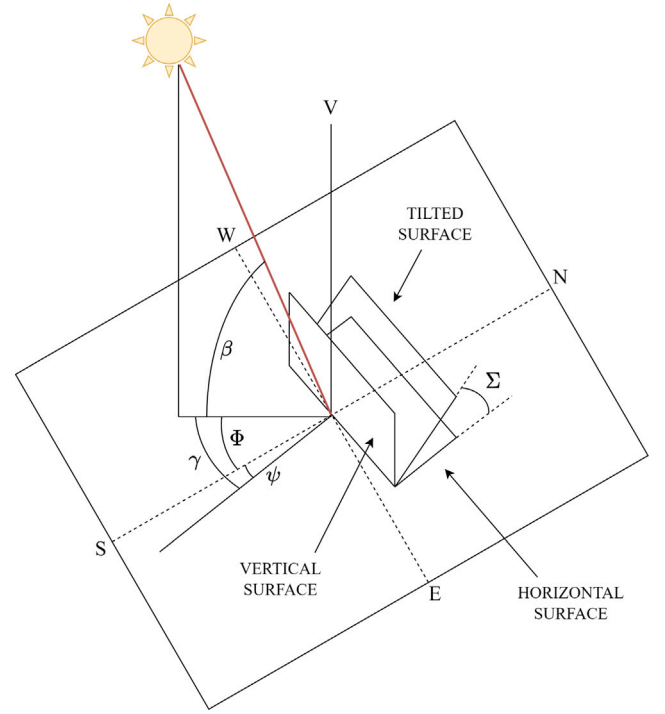

Fig. 7. Angles formed by solar radiation incident on a tilted surface.

properties of air can be estimated according to the polytropic ideal gas model, the adiabatic wall temperature can be computed as

$$T_{\text{aw}} = T_{\text{amb}} \left(1 + Pr_{\text{aw}}^{1/3} \frac{\gamma_{\text{amb}} - 1}{2} Ma_{\infty}^2 \right). \tag{25}$$

In turn, the heat flow rate reads

$$\dot{Q}_{\text{conv,ext}} = h_t A (T_{\text{fus,ext}} - T_{\text{aw}}). \tag{26}$$

During flight, the fuselage is at free-stream static pressure with a very good degree of approximation, thus the flat-plate analogy applies and the convective heat transfer coefficient can be conveniently computed as

$$h_t = 0.185 \rho^* c_P^* V_\infty \cdot (\log_{10} Re_x^*)^{-2.584} \cdot Pr^{*-2/3}, \tag{27}$$

where Re_x^* is the Reynolds number evaluated at x, that is the distance from the fuselage nose; its value is bounded between 10^7 and 10^9. In this formulation, the quantities denoted by $*$ are evaluated at the thermodynamic state defined by the ambient pressure and the temperature T^*, given by [22]

$$T^* = \frac{T_{\text{aw}} + T_{\text{amb}}}{2} + 0.22(T_{\text{aw}} - T_{\text{amb}}). \tag{28}$$

Conversely, when the aircraft is stationary on the ground, the heat flow rate due to external convection is equal to

$$\dot{Q}_{\text{conv,ext}} = h_t A (T_{\text{fus,ext}} - T_{\text{amb}}). \tag{29}$$

In the limiting case of buoyancy-driven free convection, the heat transfer coefficient can be expressed as

$$h_{t,\text{free}} = \frac{0.13 k_t (Gr \cdot Pr)^{1/3}}{D_{\text{fus,ext}}}, \tag{30}$$

where the Prandtl number is computed at the thermodynamic state f defined by the ambient pressure and the temperature T_f, given by

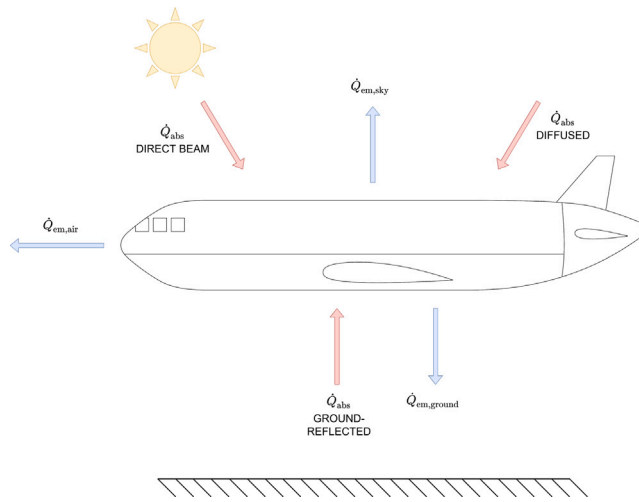$$T_f = \frac{T_{\text{fus,ext}} + T_{\text{amb}}}{2}. \tag{31}$$

Fig. 8. Absorbed and emitted components of the radiative heat transfer between the aircraft fuselage and the external environment.

Table 1
Data of the validation test cases. The aircraft under analysis is an Airbus A320. Some of the data entries are normalized to preserve confidentiality.

Test case	Hot ground	Cruise	Faulty pack
$\dfrac{\dot{m}_{ECS}}{\dot{m}_{ECS,ground}}$ [%]	100	106	88
$\dfrac{\dot{m}_{rec}}{\dot{m}_{ECS} + \dot{m}_{rec}}$ [%]	50	50	50
ϕ_{ECS}	0	0	0
T_{target} [°C]	27	24	27
z [km]	0	11.89	11.89
Ma_∞ [°C]	0	0.78	0.78
ΔT_{ISA} [°C]	23	0	16
LAT [°]	33.754	33.754	33.754
LON [°]	−84.39	−84.39	−84.39
n	200	200	200
h	12	12	12
N_{pax}	196	180	180
N_{crew}	6	6	6
N_{pilots}	3	3	3
$\dot{Q}_{el}$ [kW]	1.2	1.2	1.2
$\dot{Q}_{gal}$ [kW]	1.5	1.5	1.5
$\dot{Q}_{av}$ [kW]	10	0	0
$\dot{Q}_{cl}$ [kW]	1.15	1.15	1.15
$\dot{Q}_{ife}$ [kW]	5.88	5.40	5.40

In this context, the Grashof number is evaluated as

$$Gr = \frac{g}{T_f} \frac{|T_{fus,ext} - T_{amb}| \cdot D_{fus,ext}^3}{v_f^2}, \tag{32}$$

and the convective heat transfer correlation is valid for $10^9 < Gr \cdot Pr < 10^{12}$. In the presence of wind, forced convection is the heat transfer mechanism, and the heat transfer coefficient can be estimated as

$$h_{t,forced} = \frac{0.0266 k_{t,f} \cdot Re_f^{0.805} \cdot Pr^{1/3}}{D_{fus,ext}}. \tag{33}$$

In this expression, the Reynolds number is evaluated as

$$Re_f = \frac{\rho_f V_{wind} D_{fus,ext}}{\mu_f}, \tag{34}$$

and its value is bounded between $4 \cdot 10^4$ and $4 \cdot 10^5$.

In the case of convection heat transfer occurring between the inner surfaces of the fuselage and the air volume inside the pressurized aircraft compartments, the heat flow rate is expressed as

$$\dot{Q}_{conv,int} = h_{t,int} A(T_{int} - T_{fus,int}), \tag{35}$$

and the heat transfer coefficient can be simply computed according to [29]

$$h_{t,int} = 5.6783 \cdot (2 + 0.314 \cdot 3.2808 \cdot V_{int}), \tag{36}$$

where V_{int} can assume values up to 1 m/s in an occupied compartment.

According to this discretization method, heat transfer can be modeled with the same thermal network in the upper and lower sections of the fuselage, with exception of the heat transfer occurring in presence of transparencies, e.g., cabin windows. To account for transparent surfaces, the upper section of the fuselage is discretized with five elements, whereby the two lateral segments include suitable models for the heat transfer related to the windows. The complete thermal network used to model the upper fuselage sector corresponding to a cabin ventilation zone is displayed in Fig. 4d. The fuselage sector corresponding to the cockpit is modeled in the same fashion, with models for the lateral and frontal flight deck windshields in place of the cabin windows models.

3. Validation

In order to assess the accuracy of the thermal model of the aircraft fuselage, the simulation results have been compared with proprietary data confidentially disclosed by Airbus. The validation test cases comprise the most relevant operating points defining the design of the ECS

of an Airbus A320. The operating conditions on which the ECS design is based are: i) standard cruise conditions, ii) ground operation on a hot and humid day, and (iii) flying conditions in case of a faulty ECS pack. The characteristics of the aircraft considered for the validation test cases are reported in Table 4. Moreover, the specifications of the aircraft composite structures, cabin windows and flight deck windshields are listed in Table 5, Table 6, Table 7, and Table 8. The data related to the A320 has not been disclosed by Airbus due to confidentiality, but rather collected from different sources available in the scientific literature and in technical manuals. Therefore, the information reported in the aforementioned tables may be inaccurate or outdated. The three considered operating points are defined by the data reported in Table 1. These include:

- the total mass flow rate of fresh air provided by the ECS, together with the relative humidity at the outlet of the pack and the recirculation ratio;
- the temperature set point, assumed to be equal for all the ventilation zones;
- the altitude and speed of the aircraft;
- the data about the climate, including the geographic location, date and time, and deviation from the ISA standard conditions;
- the number of occupants onboard the aircraft, namely, passengers, crew members, and pilots;
- the thermal energy generated inside the fuselage, namely that due to flight deck electronics, avionics, galleys, in-flight entertainment, and cabin lights.

The model is used to compute the conditions at the outlet of the ECS packs required to comply with the pressure and temperature set points prescribed for each ventilation zones. The absolute deviations between the predictions of the model and the data provided by Airbus are reported in Table 2, whereas the actual values are omitted for confidentiality. The maximum absolute deviations in terms of temperature and pressure at the discharge of the ECS packs are equal to 2.4 K and 4.5 kPa, respectively. Accounting for the uncertainty in the data about the climate or external environment and the uncertainty related to the technical specifications of the aircraft, which have not been provided by Airbus, the accuracy of the model is deemed acceptable for the purpose of this study.

In addition to the absolute deviations between the model predictions and the validation data, Table 2 lists the ratio between the airflow delivered to the cockpit and cabin, as well as the total heat flow rate

Table 2
Results of the validation test cases. The aircraft under analysis is an Airbus A320. The results are normalized or expressed as deviation with respect to proprietary data to preserve confidentiality.

Test case	Hot ground	Cruise	Faulty pack
ΔT_{ECS} [°C]	2.42	1.14	0.74
ΔP_{ECS} [kPa]	0.07	0.58	4.47
$\dot{m}_{\mathrm{cpt}}/\dot{m}_{\mathrm{cab}}$ [%]	12.6	11.7	11.7
$\dot{Q}_{\mathrm{tot}}$ [kW]	n.a.	n.a.	n.a.
$\dot{Q}_{\mathrm{cpt}}/\dot{Q}_{\mathrm{tot}}$ [%]	6.8	1.8	2.7
$\dot{Q}_{\mathrm{cpt,int}}/\dot{Q}_{\mathrm{cpt}}$ [%]	45.1	266	186.9
$\dot{Q}_{\mathrm{cpt,ext}}/\dot{Q}_{\mathrm{cpt}}$ [%]	54.9	−166	−86.9
$\dot{Q}_{\mathrm{cab}}/\dot{Q}_{\mathrm{tot}}$ [%]	62.9	69.3	78.4
$\dot{Q}_{\mathrm{cab,int}}/\dot{Q}_{\mathrm{cab}}$ [%]	94.3	123.1	116.3
$\dot{Q}_{\mathrm{cab,ext}}/\dot{Q}_{\mathrm{cab}}$ [%]	5.7	−23.1	−16.3
$\dot{Q}_{\mathrm{ufloor}}/\dot{Q}_{\mathrm{tot}}$ [%]	30.3	28.9	18.9
$\dot{Q}_{\mathrm{ufloor,int}}/\dot{Q}_{\mathrm{ufloor}}$ [%]	64.6	0.0	0.0
$\dot{Q}_{\mathrm{ufloor,ext}}/\dot{Q}_{\mathrm{ufloor}}$ [%]	35.4	100	100

computed for the entire fuselage and the individual compartments, i.e., cockpit, cabin, and underfloor, comprising both cargo and E/E bays. Furthermore, these are divided into two contributions, depending on whether the corresponding thermal energy source is internal or external to the fuselage. The external heat flow rate is considered positive when entering the considered control volume. As can be noticed in Table 2, most of the thermal energy that must be removed by the ECS can be attributed to the cabin. While the aircraft is flying, part of the thermal energy coming from the sources internal to the fuselage is transferred to the external cold environment. Instead, during ground operation on a hot and humid day, the heat transfer with the environment is in the opposite direction and further increases the total heat load of the ECS. The same considerations apply to the cockpit section, with a higher relative influence of the heat transfer with the external environment, due to the relatively larger transparent surfaces. The underfloor volumes do not feature any source of thermal energy, except for the avionics. During flight, the avionics are cooled by the skin heat exchanger, therefore they are not accounted for in the model. However, the avionics heat generation must be taken into account in case of hot ground operation, the most critical operating condition, which defines the sizing point of the ECS.

4. Applications

To showcase the capabilities of the fuselage thermal model developed with the *DynTherM* library, two examples of applications are documented. The selected aircraft configuration is the same used for model validation, i.e., an Airbus A320. However, the library can be used to model the fuselage thermal fluxes of any other commercial aircraft.

4.1. ECS operating envelope

The operating envelope of the Airbus A320 ECS is identified by simulating 50 operating points, belonging to widely different operating scenarios, namely ground, climb, cruise, and faulty pack operations, and simulated at variable climate conditions. The data defining these operating points are listed in Table 3. In particular, each of the 10 selected flight phases is simulated for 5 different climate conditions. The results are displayed in Figs. 9 and 10. Fig. 9 shows that the temperature at the discharge of the ECS is almost insensitive to the change of flight phase. The only exception is ground operation, which is always characterized by higher cooling demand. Conversely, T_{ECS} strongly scales with the change of the environmental conditions, with temperature variations of up to ≈ 25°C for the same flight condition. Furthermore, the cabin pressure delivered by the ECS is only a function of the aircraft altitude, thus of the flight phase. According to industry best practices, the ECS of passenger aircraft must be sized to meet

Table 3
Data of the operating points used to identify the operating envelope of the ECS of an Airbus A320. The parameters T_{target}, z, Ma_∞, ΔT_{ISA}, n, h, N_{pax}, $\dot{Q}_{\mathrm{av}}$, $\dot{Q}_{\mathrm{ife}}$ assume different values in the range defined by the lower bound (lb) and the upper bound (ub). Some of the data entries are normalized to preserve confidentiality.

| Test case	Ground	Climb	Cruise	Faulty pack
$\dfrac{\dot{m}_{\mathrm{ECS}}}{\dot{m}_{\mathrm{ECS,ground}}}$ [%]	100	106	106	88
$\dfrac{\dot{m}_{\mathrm{rec}}}{\dot{m}_{\mathrm{ECS}}+\dot{m}_{\mathrm{rec}}}$ [%]	50	50	50	50
ϕ_{ECS}	0	0	0	0
T_{target} [°C]	24 : 27	24	24	24
z [km]	0	6 : 9	11.89	11.89
Ma_∞	0	0.6 : 0.78	0.78	0.78
ΔT_{ISA} [°C]	−23 : 23	−23 : 23	−23 : 23	−23 : 23
LAT [°]	33.754	33.754	33.754	33.754
LON [°]	−84.39	−84.39	−84.39	−84.39
n	20 : 200	20 : 200	20 : 200	20 : 200
h	9 : 12	9 : 12	9 : 12	9 : 12
N_{pax}	100 : 196	100 : 196	100 : 196	100 : 196
N_{crew}	6	6	6	6
N_{pilots}	3	3	3	3
$\dot{Q}_{\mathrm{el}}$ [kW]	1.2	1.2	1.2	1.2
$\dot{Q}_{\mathrm{gal}}$ [kW]	1.5	1.5	1.5	1.5
$\dot{Q}_{\mathrm{av}}$ [kW]	0 : 10	0	0	0
$\dot{Q}_{\mathrm{cl}}$ [kW]	1.15	1.15	1.15	1.15
$\dot{Q}_{\mathrm{ife}}$ [kW]	0 : 5.88	0 : 5.88	0 : 5.88	0 : 5.88
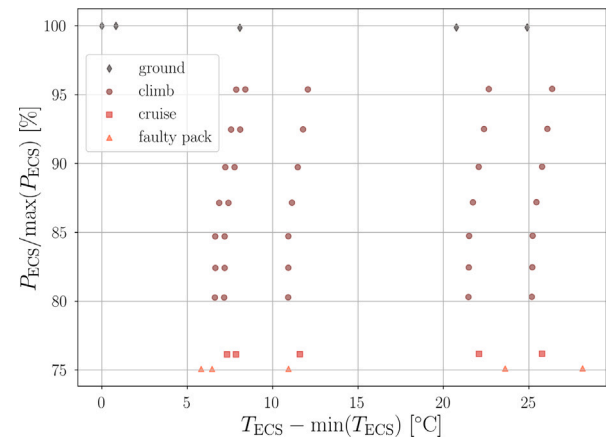
Fig. 9. Operating envelope of the ECS of an Airbus A320 in terms of pressure and temperature at the pack discharge calculated with the fuselage thermal model. The results are normalized or expressed as absolute differences to preserve confidentiality.

Table 4
General dimensions of an Airbus A320 [5,30–32].

Cockpit		Cabin		Underfloor	
R_{cpt} [m]	2.07	R_{cab} [m]	2.07	$L_{\mathrm{cargo,fwd}}$ [m]	4.95
L_{cpt} [m]	3.5	L_{cab} [m]	26.9	$L_{\mathrm{cargo,aft}}$ [m]	9.8
V_{cpt} [m³]	9	V_{cab} [m³]	139	L_{EEbay} [m]	4
$A_{\mathrm{cpt,int}}$ [m²]	8	$A_{\mathrm{cab,int}}$ [m²]	360	$V_{\mathrm{cargo,fwd}}$ [m³]	15.56
$m_{\mathrm{cpt,int}}$ [kg]	80	$m_{\mathrm{cab,int}}$ [kg]	3600	$V_{\mathrm{cargo,aft}}$ [m³]	20.77
$c_{\mathrm{cpt,int}}$ [J/kg]	1000	$c_{\mathrm{cab,int}}$ [J/kg]	1000	V_{EEbay} [m³]	9
$L_{\mathrm{pipe,cpt}}$ [m]	13.45	$L_{\mathrm{pipe,cab}}$ [m]	13.45	H_{floor} [m]	1.3
$D_{\mathrm{pipe,cpt}}$ [m]	0.08	$D_{\mathrm{pipe,cab}}$ [m]	0.18		
$L_{\mathrm{wshield,f}}$ [m]	2.08	L_{wind} [m]	0.23		
$L_{\mathrm{wshield,l}}$ [m]	1.32	H_{wind} [m]	0.33		
$H_{\mathrm{wshield,f}}$ [m]	0.5	N_{wind} [-]	60		
$H_{\mathrm{wshield,l}}$ [m]	0.5				

the extreme operating points of the envelope. At the same time, the ECS should be optimized for the most common operating conditions. Therefore, the information displayed in the $P − T$ diagram of Fig. 9, together with the corresponding mass flow rate of fresh air provided for each operating point, is essential to tackle the multi-point design optimization of the system.
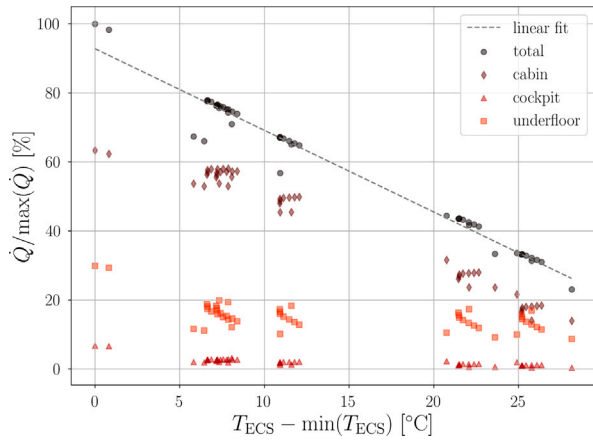
Fig. 10. Total and individual components of the heat load displayed as a function of the pack discharge temperature for the ECS operating points of an Airbus A320 calculated with the fuselage thermal model. The results are normalized or expressed as absolute differences to preserve confidentiality.

Table 5
Dimensions and material properties of the fuselage composite structure of an Airbus A320 [33,34].

Parameter	Skin	Skin core	Insulation
Material	Carbon phenolic	Hexcel HRH-10-1/8-6.0	Glass fiber
t [mm]	1.36	12.0	80.28
ρ [kg m^{-3}]	1800	93	9.6
k_t [W m^{-1} K^{-1}]	1.0	0.068	0.036
c [J kg^{-1} K^{-1}]	600	1300	1005

Parameter	Int. panel	Int. panel core	
Material	Glass phenolic	Fibrelam 1100 HRH-10-1/8-4.0	
t [mm]	0.5	4.0	
ρ [kg m^{-3}]	2550	64	
k_t [W m^{-1} K^{-1}]	0.24	0.0675	
c [J kg^{-1} K^{-1}]	1110	1300	

Table 6
Dimensions and material properties of the floor and cabin wall composite structures of an Airbus A320 [33,34].

Parameter	Panel	Core
Material	Carbon phenolic	Fibrelam 6100 HRH-10-1/8-9.0
t [mm]	0.762	23.88
ρ [kg m^{-3}]	1800	139
k_t [W m^{-1} K^{-1}]	1.0	0.0675
c [J kg^{-1} K^{-1}]	600	1300

Table 7
Dimensions and material properties of the flight deck windshield of an Airbus A320.

Parameter	Glass shield	Outer panel	Inner panel
Material	Tempered glass	Opticor	Opticor
t [mm]	5.0	20.0	25.0
ρ [kg m^{-3}]	2500	1130	1130
k_t [W m^{-1} K^{-1}]	0.8	0.21	0.21
c [J kg^{-1} K^{-1}]	800	840	840
n [-]	1.47	1.52	1.52
τ [-]	0.918	0.9	0.9

The characterization of the operating envelope is complemented by Fig. 10, where the temperature of the fresh air at the pack discharge is correlated with the total thermal load, as well as with the individual components related to the cabin, cockpit, and underfloor compartments. In accordance with what reported in Section 3, the

Table 8
Dimensions and material properties of the cabin windows of an Airbus A320.

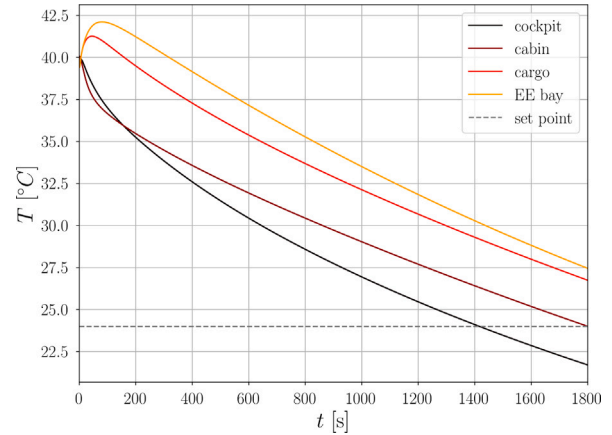| Parameter	Outer panel	Air cavity	Inner panel
Material	Opticor	Air	Opticor
t [mm]	10.0	7.0	5.0
ρ [kg m^{-3}]	1130	–	1130
k_t [W m^{-1} K^{-1}]	0.21	–	0.21
c [J kg^{-1} K^{-1}]	840	–	840
n [-]	1.52	–	1.52
τ [-]	0.9	–	0.9

Fig. 11. Pull-down case study: temporal evolution of the temperature in the main aircraft compartments computed with the Airbus A320 fuselage thermal model obtained with the *DynTherM* library.

cabin is responsible for the largest share of the ECS duty, followed by the underfloor areas, and the cockpit. Interestingly, the relationship between T_{ECS} and the total heat load can be approximated by linear regression with good accuracy. For this example, the linear correlation reads

$$\dot{Q}_{tot} = 31.028 - 1.227 T_{ECS}, \tag{37}$$

where $\dot{Q}_{tot}$ and T_{ECS} are expressed in kilowatt and degree Celsius, respectively. In turn, if an estimate of the total heat load related to another operating point is available, this simple equation can be used to compute a first guess of the temperature at the ECS discharge, or vice versa. This approach is significantly less time-consuming than setting up a new test case and running the fuselage thermal model, thus it can be conveniently used to assess the ECS operating envelope during the preliminary design phase. However, this correlation cannot be generalized to a different aircraft configuration.

4.2. Pull-down operating point

This case study is concerned with the simulation of a pull-down operating point, i.e., an operating condition for which the aircraft is on the ground on a hot day, but empty of passengers, and with minimal heat loads internal to the fuselage. The initial temperature is set to 40 °C in all the ventilation zones and the ECS must lower it to the set point of 24 °C within 30 min. Differently from the operating conditions analyzed in Sections 3 and 4.1, which require only steady-state simulations, this test case is about the dynamics of the system. The pull-down operating point is included in the requirements for the certification of the ECS. Therefore, the accurate simulation of the ECS dynamics is of paramount importance.

The simulation setup is similar to the one used for the hot ground case reported in Table 1. The only differences are the absence of passengers in the cabin, the absence of thermal energy input due to galleys, avionics, and in-flight entertainment, and the lower value of
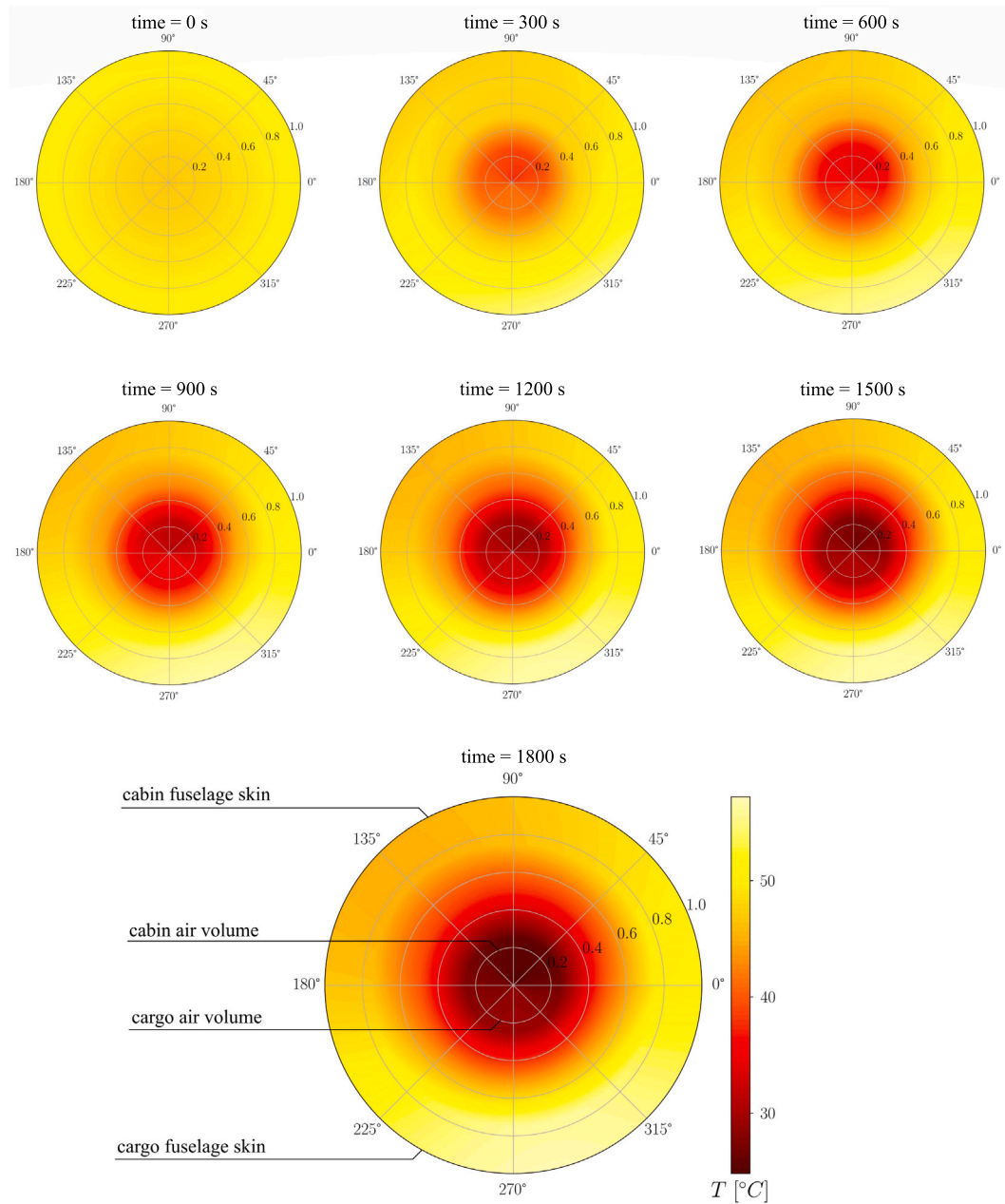
Fig. 12. Pull-down case study: temperature distribution in the cabin and cargo compartments computed at different time instants using the Airbus A320 fuselage thermal model implemented with the *DynTherM* library. The fuselage is discretized with eight elements along the circumferential direction. The inner section of the polar plot corresponds to the pressurized air volumes, whereas the outer section represents the fuselage skin.

recirculation ratio, set to 20%. The temperature at the outlet of the ECS pack is set to $T_{\mathrm{ECS}} = -15°C$. The following considerations can be drawn from the results displayed in Fig. 11. First, the ECS is capable of meeting the temperature set point of 24 °C in the prescribed time for both ventilation zones. In the absence of trim air and active control of the airflow delivered to the different ventilation zones, the cockpit reaches the temperature set point in approximately 23.3 min, whereas the cabin requires 30 min, due to its higher thermal inertia. Moreover, a temperature rise is observed in the underfloor compartments during the initial transient. To explain this phenomenon, it is important to notice that the initial temperature has been set to the same value in all the ventilation zones without accounting for thermal equilibrium. An alternative approach to avoid the initial temperature rise in the underfloor compartments consists in using the results of a steady-state simulation without the ECS to initialize the transient simulation of the pull-down case.

Additional insights about the time-dependent evolution of the temperature distribution in the cabin and cargo compartments can be gained by analyzing Fig. 12. In accordance with what documented in Section 2 and displayed in Fig. 2, the fuselage is discretized with eight elements along the circumferential direction. Each element is a circular sector of the composite structure described in Section 2.3, featuring the properties reported in Table 5. The temperature of the air in the cabin and cargo volumes is displayed in the central part of the polar plot. The outer portion of the polar plot corresponds to the fuselage skin. In between them, the temperature distribution is shown for the different portions of the fuselage composite structure.

At the initial time instant of the simulation, the temperature is uniform and equal to the prescribed initial condition of 40 °C. Afterwards, the simulation evolves with the injection of a mixture of fresh and recirculated air into the cabin and a radial temperature gradient

is progressively established between the internal air volume and the fuselage skin. At the same time, the conditioned air is circulated to the cargo bay by means of the dado panels located on the cabin floor, leading to a higher temperature in the lower sections of the fuselage. At the last time instant, the highest temperature, i.e., 56.9 °C, is measured in the lower right part of the fuselage skin, whereas the coldest portion of the skin, i.e., 43.6 °C, is located in the opposite corner. At the same locations, the radial temperature gradient evaluated through the fuselage composite structure is equal to 30.1 °C and 19.6 °C, respectively. This highlights the presence of a non-symmetric solar radiation field acting on the fuselage at the specified climate conditions. Moreover, the non-uniformity shows the influence of ground-reflected solar radiation and ground-emitted radiation on the fuselage temperature distribution when operating the aircraft on the ground during a hot day. This information can be used to assess the influence of the layout and the materials used for the fuselage composite structure on the thermal dynamics of the aircraft.

5. Conclusions

This paper documents the development, validation, and application of the *DynTherM* Modelica library. The modules of this library allow to build the dynamic thermal model of the air distribution system and the pressurized compartments of a passenger aircraft. The model has been validated with proprietary data concerning the fuselage thermal characteristics of an Airbus A320 provided by the aircraft manufacturer. For the considered validation case studies, the results computed by the model show maximum absolute deviations of 2.4 K and 4.5 kPa with respect to the actual temperature and pressure evaluated at the discharge of the ECS pack. Differently from previous research efforts documented in the scientific literature, the *DynTherM* library and the associated fuselage thermal model are released open-source under the GNU General Public License, to promote the reproducibility of results and the open dissemination of knowledge. The validated thermal model has been used to compute the operating envelope of the ECS of an Airbus A320. The outcomes show that the thermodynamic state at the discharge of the pack varies substantially as a function of the flight phase and climate conditions. This confirms the need for a fast and accurate thermal model to provide the specifications for the multi-point design optimization of a novel ECS configuration. Finally, the study is complemented with the simulation of a test case involving a pull-down operating point. The results reveal the ability of the model to capture the dynamic thermal behavior of the system and provide additional insights about the evolution of the temperature distribution throughout the different sections of the fuselage as a function of time. These results are of paramount importance for future sustainable aircraft, whose ECS should be re-designed to exploit possible synergies with other onboard thermal management systems.

Currently, the modeling method at the basis of the *DynTherM* library is affected by the following limitations:

- the leakage of pressurized air through the fuselage is neglected, leading to a possible underestimation of the ECS pressurization requirements;
- the heat transfer through the fuselage is modeled as one dimensional, i.e., only heat transfer along the radial direction is considered, as the thermal resistance in the circumferential direction is negligible if compared to the radial one. However, to simulate more accurately the temperature distribution in the presence of a non-symmetric solar field, also the heat transfer in the circumferential direction must be modeled, at the expenses of increased complexity and computational cost;
- the temperature at the ECS pack discharge is computed to match the temperature set point in one ventilation zone, e.g., the cabin. Then the trim air flow rate is prescribed to achieve the set temperature in the remaining ventilation zones, e.g., the cockpit.

To simplify the use of the model, it is necessary to automatically vary the opening of the trim air valves to match the temperature set point in all the ventilation zones.

Future work will entail the study of non-conventional ECS architectures for aircraft configurations alternative to the Airbus A320. For this purpose, the dynamic thermal model of the aircraft fuselage will be tailored for each aircraft configuration and applied to retrieve the corresponding ECS operating envelope. A similar study will be performed for large rotorcraft applications. Moreover, future research will target the development of thermal management systems for disruptive aircraft layouts, aimed at accelerating the transition to net zero emissions by the aviation sector, such as battery-powered and fuel cell-powered aircraft. To tackle the design of such systems, the *DynTherM* library will be extended to include models for characterizing the dynamic thermal behavior of battery packs, as well as that of hydrogen storage and distribution systems.

Metadata

The *DynTherM* Modelica library is distributed under the GNU General Public License and can be freely downloaded at the following link:

https://github.com/Propulsion-Power-TU-Delft/DynTherM

CRediT authorship contribution statement

Andrea Giuffre': Conceptualization, Data curation, Methodology, Software, Validation, Writing – original draft. **Piero Colonna:** Funding acquisition, Supervision, Writing – review & editing. **Carlo De Servi:** Conceptualization, Funding acquisition, Methodology, Supervision, Writing – review & editing.

Declaration of competing interest

The authors declare that they have no known competing financial interests or personal relationships that could have appeared to influence the work reported in this paper.

Data availability

The software is released open-source and the link to the online repository is included in the paper. The remaining data are confidential.

Appendix A. Solar radiation

The solar constant E_{sc} is defined as the intensity of solar radiation acting on a surface normal to the sun's rays at the average earth–sun distance, and is equal to $E_{sc} = 1367$ W m^{-2} [35]. The extraterrestrial radiant flux E_0 varies throughout the year since the earth's orbit is slightly elliptical. Its value can be approximated as

$$E_0 = E_{sc} \left(1 + 0.033 \cos \left(2\pi \frac{n-3}{365} \right) \right), \tag{38}$$

where *n* is the day of the year. The earth's orbital velocity also varies throughout the year, so the apparent solar time (AST) varies from the

time measured by a clock running at a uniform rate. This variation is quantified by the equation of time (ET), which reads

$$ET = 2.2918(0.0075 + 0.1868 \cos \Gamma - 3.2077 \sin \Gamma + \\ - 1.4615 \cos 2\Gamma - 4.089 \sin 2\Gamma),$$
(39)

where ET is expressed in minutes and

$$\Gamma = 360° \frac{n-1}{365}.$$
(40)

The conversion between Local Standard Time (LST) and apparent solar time involves also a longitude correction. This corresponds to four minutes per degree difference between the local site longitude and the longitude of the Local Standard Meridian (LSM) for the prescribed time zone. Hence, the AST can be computed as

$$AST = LST + \frac{ET}{60} + \frac{LON - LSM}{15}.$$
(41)

The angle between the earth/sun line and the equatorial plane, called solar declination δ, varies throughout the year since the earth's equatorial plane is tilted with respect to the orbital plane. For most engineering applications, it can be approximated as

$$\delta = 23.45° \sin \left(360° \frac{n+284}{365} \right).$$
(42)

The sun's position in the sky can be conveniently expressed in terms of solar altitude and azimuth. With reference to Fig. 7, the solar altitude angle β is defined as the angle between the horizontal plane and a line emanating from the sun. Its value ranges from 0° when the sun is on the horizon, to 90° if the sun is directly overhead. The solar azimuth angle Φ is defined as the angular displacement from the south of the horizontal projection of the earth/sun line. The solar altitude and azimuth angles depend on the local latitude LAT, the solar declination δ, and the hour angle H, expressed as

$$H = 15(AST - 12).$$
(43)

The azimuth angle is uniquely determined by its sine and cosine, given by

$$\sin \Phi = \frac{\cos \delta \sin H}{\cos \beta},$$
$$\cos \Phi = \frac{\cos \delta \cos H \sin LAT - \sin \delta \cos LAT}{\cos \beta}.$$
(44)

Solar radiation on a clear day is defined by its direct component, i.e., the radiation emanating directly from the solar disc, and its diffuse component, i.e., the radiation emanating from the rest of the sky. These two components are calculated as

$$E_b = E_0 e^{-\tau_b m^{ab}},$$
$$E_d = E_0 e^{-\tau_d m^{ad}}.$$
(45)

Values of τ_b and τ_d are location-specific, and vary during the year. They embody the dependence of clear-sky solar radiation on local conditions, such as elevation, precipitable water content, and aerosols. Their average values have been determined at prescribed locations through ASHRAE research projects RP-1453 [36] and RP-1613 [37]. Air mass exponents ab and ad are correlated to τ_b and τ_d through the following empirical relationships

$$ab = 1.454 - 0.406\tau_b - 0.268\tau_d + 0.021\tau_b\tau_d,$$
$$ad = 0.507 + 0.205\tau_b - 0.080\tau_d - 0.190\tau_b\tau_d.$$
(46)

The relative air mass m corresponds to the ratio between the mass of the air column in the actual earth/sun path and the one computed assuming that the sun is directly overhead. It can be computed according to [38]

$$m_0 = \frac{1}{\sin \beta + 0.50572(6.07995 + \beta)^{-1.6364}},$$
(47)

where the subscript 0 indicates that the receiving object is at ground level. Conversely, if the receiver is flying at high altitude, the relative air mass must be corrected as follows [39]

$$m = m_0 \left(\frac{T_{amb} - 0.0065z}{T_{amb}} \right)^{5.2561}.$$
(48)

The orientation of a receiving surface is characterized by the tilt angle and azimuth. The tilt angle Σ is the angle between the surface and the horizontal plane. A value of 0° corresponds to a horizontal plane, whereas a value of 90° represents a vertical surface. The surface azimuth ψ is defined in the same fashion as for the sun's position. Surfaces that face west have a positive surface azimuth; those that face east have a negative surface azimuth. The surface-solar azimuth angle γ is defined as the angular difference between the solar azimuth and the surface azimuth: $\gamma = \Phi - \psi$. Values of γ greater than 90° or lower than −90° indicate that the surface is in the shade. Finally, the angle between the earth–sun line and the normal to the irradiated surface is called the incidence angle and is computed as

$$\cos \theta = \cos \beta \cos \gamma \sin \Sigma + \sin \beta \cos \Sigma.$$
(49)

The total clear-sky irradiance reaching the receiving surface can be expressed as the sum of three components: the beam component $E_{t,b}$ originating from the solar disc, the diffuse component $E_{t,d}$, originating from the sky dome, and the ground-reflected component $E_{t,r}$ originating from the ground in front of the receiving surface

$$E_t = E_{t,b} + E_{t,d} + E_{t,r}.$$
(50)

Once the incidence angle is known, the beam component can be simply computed as

$$E_{t,b} = E_b \cos \theta.$$
(51)

If $\cos \theta \leq 0$, the beam component is null. The diffuse component is more difficult to estimate because of the non-isotropic nature of the diffuse radiation. For vertical surfaces, it can be approximated according to [40]

$$E_{t,d} = E_d Y,$$
(52)

where

$$Y = \max (0.45, \ 0.55 + 0.437 \cos \theta + 0.313 \cos^2 \theta).$$
(53)

For a non-vertical surface, the diffuse component can be approximated with the following simplified relationships

$$E_{t,d} = E_d(Y \sin \Sigma + \cos \Sigma) \quad \text{if } \Sigma \leq 90°,$$
$$E_{t,d} = E_d Y \sin \Sigma \quad \text{if } \Sigma > 90°,$$
(54)

where Y is calculated for a vertical surface having the same azimuth as the prescribed receiving surface. Finally, the ground-reflected irradiance for surfaces of all orientations is given by

$$E_{t,r} = \rho_g(E_b \sin \beta + E_d) \frac{1 - \cos \Sigma}{2},$$
(55)

where ρ_g is the ground reflectance.

References

[1] M. Dechow, C. Nurcombe, Aircraft environmental control systems, in: M. Hocking (Ed.), Air Quality in Airplane Cabins and Similar Enclosed Spaces, Springer Berlin Heidelberg, Berlin, Heidelberg, 2005, pp. 3–24, http://dx.doi.org/10.1007/b107234.

[2] A. Pollok, Modelling and Control of Aircraft Environmental Control Systems (Ph.D. thesis), Politecnico di Milano, 2018.

[3] C. Giaconia, A. Orioli, A. Di Gangi, Air quality and relative humidity in commercial aircrafts: An experimental investigation on short-haul domestic flights, Build. Environ. 67 (2013) 69–81, http://dx.doi.org/10.1016/j.buildenv.2013.05.006.

[4] B. Oehler, Modeling and simulation of global thermal and fluid effects in an aircraft fuselage, in: 4th International Modelica Conference, Harburg, Germany, 2005, pp. 497–506.

[5] C. Müller, D. Scholz, T. Giese, Dynamic simulation of innovative aircraft air conditioning, in: 1st CEAS European Air and Space Conference, 2007.

[6] A. Pollok, D. Bender, I. Kerling, D. Zimmer, Rapid development of an aircraft cabin temperature regulation concept, in: 12th International Modelica Conference, 2017, pp. 151–159, http://dx.doi.org/10.3384/ecp17132151.

[7] M.A. Fayazbakhsh, M. Bahrami, Comprehensive modeling of vehicle air conditioning loads using heat balance method, SAE Tech. Pap. (2013) http://dx.doi.org/10.4271/2013-01-1507.

[8] F. Brèque, M. Nemer, Cabin Thermal Needs: Modeling and Assumption Analysis, in: Proceedings of the 12th International Modelica Conference, Prague, Czech Republic, 2017, pp. 771–781, http://dx.doi.org/10.3384/ecp17132771.

[9] M. Geron, C. Butler, J. Stafford, D. Newport, Development and validation of a compact thermal model for an aircraft compartment, Appl. Therm. Eng. 61 (2) (2013) 65–74, http://dx.doi.org/10.1016/j.applthermaleng.2013.07.012.

[10] G. Schweiger, H. Nilsson, J. Schoeggl, W. Birk, A. Posch, Modeling and simulation of large-scale systems: A systematic comparison of modeling paradigms, Appl. Math. Comput. 365 (2020) http://dx.doi.org/10.1016/J.AMC.2019.124713.

[11] The Modelica Association, Modelica 4.0, URL: https://modelica.org/.

[12] F. Casella, A. Leva, Modelica open library for power plant simulation: design and experimental validation, in: P. Fritzson (Ed.), Proceedings of the 3rd International Modelica Conference, Linköping, 2003, pp. 41–50.

[13] F. Casella, A. Leva, Modelling of thermo-hydraulic power generation processes using Modelica, Math. Comput. Model. Dyn. Syst. 12 (1) (2006) 19–33, http://dx.doi.org/10.1080/13873950500071082.

[14] P.O. Fanger, et al., Thermal Comfort. Analysis and Applications in Environmental Engineering, McGraw-Hill, 1970.

[15] ASHRAE, Thermal comfort, in: ASHRAE Handbook - Fundamentals, American Society of Heating, Refrigerating and Air-Conditioning Engineers, 2013.

[16] F. Rohles, R. Nevins, The nature of thermal comfort for sedentary man, ASHRAE Trans. 77 (1) (1971) 239–246.

[17] ISO 2533:1975, Standard Atmosphere, Standard, International Organization for Standardization, Geneva, CH, 1975.

[18] X.D. Fang, Study on saturated water-vapor pressure equations for calculation of aircraft air-conditioning systems, J. Aerosp. Power 10 (3) (1995) 299–316.

[19] Q. Dai, X. Fang, A new model for atmospheric radiation under clear sky condition at various altitudes, Adv. Space Res. 54 (6) (2014) 1044–1048, http://dx.doi.org/10.1016/j.asr.2014.05.028.

[20] F. Zanghirella, M. Perino, V. Serra, A numerical model to evaluate the thermal behaviour of active transparent façades, Energy Build. 43 (5) (2011) 1123–1138, http://dx.doi.org/10.1016/j.enbuild.2010.08.031.

[21] J.L. Wright, A correlation to quantify convective heat transfer between vertical window glazings, ASHRAE Trans. 102 (1) (1996) 940–946.

[22] ASHRAE, Climatic design information, in: ASHRAE Handbook - Fundamentals, American Society of Heating, Refrigerating and Air-Conditioning Engineers, 2013.

[23] G. Comini, S. Savino, La Captazione dell'Energia Solare, International Center for Mechanical Sciences, Udine, 2013.

[24] C.A. Gueymard, SMARTS2, A Simple Model of the Atmospheric Radiative Transfer of Sunshine: Algorithms and performance assessment, Technical Report, 1995.

[25] C.A. Gueymard, Parameterized transmittance model for direct beam and circumsolar spectral irradiance, Sol. Energy 71 (5) (2001) 325–346, http://dx.doi.org/10.1016/S0038-092X(01)00054-8.

[26] C.A. Gueymard, Interdisciplinary applications of a versatile spectral solar irradiance model: A review, Energy 30 (9) (2005) 1551–1576, http://dx.doi.org/10.1016/j.energy.2004.04.032.

[27] F. Goia, M. Perino, M. Haase, A numerical model to evaluate the thermal behaviour of PCM glazing system configurations, Energy Build. 54 (2012) 141–153, http://dx.doi.org/10.1016/j.enbuild.2012.07.036.

[28] ASHRAE, Aircraft, in: ASHRAE Handbook - Heating, Ventilating, and Air-Conditioning Applications, American Society of Heating, Refrigerating and Air-Conditioning Engineers, 2019.

[29] SAE, AIR1168/3 - Aerothermodynamic Systems Engineering and Design, Standard, SAE Aerospace, 2011.

[30] Airbus, A319/A320/A321 Flight deck and systems briefing for pilots, 1998.

[31] Airbus, A320: Aircraft characteristics airport and maintenance planning, 2020.

[32] LTU International Airways, Airbus A320/A321 ground operations manual: Aircraft data, limitation and description, 2015.

[33] L. Krakers, Parametric Fuselage Design: Integration of Mechanics and Acoustic and Thermal Insulation (Ph.D. thesis), Delft University of Technology, 2009.

[34] D. Petersen, R. Rolfes, R. Zimmermann, Thermo-mechanical design aspects for primary composite structures of large transport aircraft, Aerosp. Sci. Technol. 5 (2) (2001) 135–146, http://dx.doi.org/10.1016/S1270-9638(00)01089-0.

[35] M. Iqbal, Chapter 3 - The solar constant and its spectral distribution, in: An Introduction to Solar Radiation, Academic Press, 1983, pp. 43–58, http://dx.doi.org/10.1016/B978-0-12-373750-2.50008-2.

[36] D. Thevenard, Updating the ASHRAE Climatic Data for Design and Standards (RP-1453), Technical Report, ASHRAE, 2009.

[37] D. Thevenard, C.A. Gueymard, Updating Climatic Design Data in the 2013 ASHRAE Handbook—Fundamentals (RP-1613), Technical Report, ASHRAE, 2009.

[38] F. Kasten, A.T. Young, Revised optical air mass tables and approximation formula, Appl. Opt. 28 (22) (1989) 4735–4738, http://dx.doi.org/10.1364/AO.28.004735.

[39] G.S. Aglietti, S. Redi, A.R. Tatnall, T. Markvart, Harnessing high-altitude solar power, IEEE Trans. Energy Convers. 24 (2) (2009) 442–451, http://dx.doi.org/10.1109/TEC.2009.2016026.

[40] D. Stephenson, Equations for solar heat gain through windows, Sol. Energy 9 (2) (1965) 81–86, http://dx.doi.org/10.1016/0038-092X(65)90207-0.